



**A finite deformation theory of desolvation and swelling in partially photo-cross-linked polymer networks for 3D/4D printing applications**

Journal:	<i>Soft Matter</i>
Manuscript ID	SM-ART-11-2018-002427.R1
Article Type:	Paper
Date Submitted by the Author:	02-Jan-2019
Complete List of Authors:	Zhao, Zeang; Peking University, State Key Laboratory for Turbulence and Complex Systems & Center for Applied Physics and Technology, College of Engineering Qi, H.; Georgia Institute of Technology, School of Mechanical Engineering Fang, Daining; Peking University, State Key Laboratory for Turbulence and Complex Systems & Center for Applied Physics and Technology, College of Engineering; Beijing Institute of Technology, Institute of Advanced Structure Technology

**A finite deformation theory of desolvation and swelling in partially photo-cross-linked polymer networks for 3D/4D printing applications**

Zeang Zhao<sup>1,2</sup>, H. Jerry Qi<sup>2\*</sup>, Daining Fang<sup>1,3\*</sup>

<sup>1</sup>State Key Laboratory for Turbulence and Complex Systems & Center for Applied Physics and Technology, College of Engineering, Peking University, Beijing, 100871, P. R. China

<sup>2</sup>The George W. Woodruff School of Mechanical Engineering, Georgia Institute of Technology, Atlanta, GA 30332, USA

<sup>3</sup>Institute of Advanced Structure Technology, Beijing Institute of Technology, Beijing, 100081, P. R. China

\*Author to whom correspondence should be addressed: H.J. Qi: [qih@me.gatech.edu](mailto:qih@me.gatech.edu), D. Fang: [fangdn@pku.edu.cn](mailto:fangdn@pku.edu.cn), or [fangdn@bit.edu.cn](mailto:fangdn@bit.edu.cn)

**Abstract**

Photopolymerization is a process strongly depending on the light field in the resin. This typically results in a non-uniformly crosslinked network where some parts of the network are fully cross-linked while other parts are partially crosslinked. The partially crosslinked part could exhibit a high volume expansion upon swelling and a high volume shrinkage upon desolvation. Through a control over the light field in the photopolymer resin, this feature has been used to create solvent responsive shape changing structures as well as 3D/4D printed smart devices, showing promising application potentials. In this paper, we develop a finite deformation theory to consider the nonuniform crosslink density of the network and the interaction between different species inside the network. The mechanical properties of the network are correlated with the reaction process and the existence of residual uncrosslinked monomer is included in the partially crosslinked network. The efficiency of the theory is proved by the finite element simulations of two special applications of the partially crosslinked network.

## 1. Introduction

Active polymer based on swelling/deswelling is an attractive element for smart devices. Upon immersion in a specific solvent, significant volume expansion arises in the polymer network, which drives the shape change of the overall structure. Inspired by this phenomenon, researchers have realized several types of solvent responsive soft robotics [1], biomedical devices [2-4], multifunctional metamaterials [5, 6], as well as 3D/4D printed polymer structures [7-10]. In the aforementioned examples, the solvent responsive polymers were typically assembled together with the non-swelling support material, and the strain mismatch upon swelling drives the structure to deform. Recently, to make things easier, swelling induced shape changing were achieved by using a single type of polymer with spatial variations of crosslink density [11, 12]. The idea was further applied to surface patterning[13] and 4D printing based on Digital Light Processing (DLP)[14-16].

When monomer chains are immersed in good solvents, they disperse uniformly in the liquid and a monomer solution is created [17]. If some of the monomer chains are cross-linked to form a polymer network, although the un-crosslinked chains can still be dissolved, the cross-linked network cannot be destroyed. Constrained by the crosslink points, the network can only swell and expand. With the increase of crosslink density, the swelling ability of the cross-linked network is reduced, while fewer free chains remain to be dissolved [18, 19]. Clearly, considering the swelling of partially crosslinked polymer network, three species should be included in the thermodynamic system, which are the crosslinked network, the free uncross-linked chains and the liquid

molecules.

As a special case of the aforementioned ternary thermodynamic system, the system containing a fully cross-linked polymer network and the liquid solvent has been widely investigated in the past. In this case, there does not exist free monomer chains that can be dissolved into the solvent. From the theoretical point of view, the research on the interaction between polymer network and swelling solvent can be dated back to the pioneering works of Gibbs[20], Flory[21] and Biot[22]. Following the idea of Gibbs and Biot, Hong et al[23] established the coupled theory of swelling gels in terms of nonequilibrium thermodynamics, Duda et al[24] proposed the finite deformation theory that is applicable to arbitrary boundary conditions, Chester et al[25] established the mechanical framework considering the non-Gaussian nature of the polymer network. Later on, the mechanical framework was further improved and completed for the applications in different types of gels and polymers, for example the temperature responsive gels[26, 27], the pH responsive gels[28], the self-healing gels[29], the interpenetrating networks[30] and the light activated polymers[31, 32]. In order to obtain the theoretical and numerical analysis of specific conditions in the swelling of polymer networks, Hong et al[33] implemented the coupled theory in the commercial finite element analysis (FEA) software ABAQUS by using the user-defined hyperelastic material; Duan et al[34] simulated the transient swelling behavior of gels based on the analogy between diffusion and heat transfer; Chester et al[35] and Bouklas et al[36] developed their own novel elements to deal with the coupling between diffusion and large deformation.

The aforementioned theories and numerical methods have shown their efficiency in the design and analysis of the network/solvent system [2, 8, 37]. However, in many real applications, the conditions are more complicated. During the photo-crosslinking of resin solution (which is finished by shining light on the liquid oligomers and monomers [38, 39]), because of the nonuniform light absorption, the resultant crosslink density of the network can be nonuniform. Some parts of the network are fully cross-linked, while other parts are only partially cross-linked. When this nonuniform network is immersed in solvent, the free monomer chains in the partially photo-crosslinked network dissolve into the solvent, and the network will be swollen. In addition, if the free monomer chains and the solvent are cleaned away from the network (namely the desolvation process), the remaining product will be the dry network (which means there is no free moving species inside the network) with nonuniform crosslink density. The nonuniform swelling leads to different expansion ratios in the network, while the nonuniform desolvation leads to different shrinkage ratios. Based on this phenomenon, researchers have realized the shape transformation of differentially photo-cross-linked polymer films. By controlling the light patterns in photopolymerization, the spatial distribution of crosslink density can be regulated, and the polymer films deforms to complex 3D shapes upon desolvation and swelling[11, 12, 16, 40].

Because of the complexity of the ternary thermodynamic system, most of the previous researches in this field were limited to experimental verifications. Some researchers simulated the surface instability[41] and shape transformation[16] of partially photo-crosslinked polymers using the classical theory of network/solvent

system. However, the existence of un-crosslinked monomer chains could not be included in the simulations, and the nonuniform crosslink density in the network was implemented empirically without investigating the underlying chemical reactions. In this paper, we propose a theoretical framework that can describe the desolvation and swelling of the partially photo-cross-linked network at the same time. The theory couples structure inhomogeneity due to incomplete chemical reactions, the swelling and shrinking behavior of this inhomogeneous network, and mechanical deformation, with the application toward 3D/4D printing. Considering the finite deformation of the network, the nonuniform crosslink density in the network and the migration of different species during desolvation and swelling, a new type of free energy function of the ternary system is proposed. The nonuniform crosslink density of the network is predicted by tracking the reaction photopolymerization kinetics of monomer chains. The efficiency of the theory is demonstrated by several FEA simulations of the desolvation/swelling induced shape changing structures.

## **2. Models**

### **2.1. Reaction kinetics of photo-crosslinking**

Upon irradiation by light of specific wavelength, photo-crosslinkable resins consisting of short chain monomers react to form a network. Here we are interested in the free-radical photopolymerization, in which the reaction is triggered by the generation of free-radicals under light irradiation[39]. These free radicals break the acrylate C=C double bonds in the resin (as shown in Fig. 1), and these bonds connect to form long chains and crosslink points. As a result, the degree of the photo-crosslink

reaction can be determined by measuring the amount of the remaining double bonds in the network[42]. The double bonds in the un-crosslinked monomer chains are unbroken, and these chains should be identical to the monomer chains in the fresh unreacted resin. For simplicity, the degree of conversion (DoC) of the double bonds can be defined as a scalar value,  $p$ , in the range from 0 to 1, which indicates the liquid resin and the fully cross-linked network, respectively. We also assume that for an arbitrary point in the material,  $p$  is independent of the choice of deformation configuration. The evolution of DoC during photopolymerization can be described by the simple kinetic model [43],

$$\frac{\partial p(\mathbf{X}, t)}{\partial t} = K_r (1 - p(\mathbf{X}, t)) I(\mathbf{X}, t), \quad (1)$$

where  $t$  is the reaction time,  $K_r$  is the reaction coefficient,  $\mathbf{X} = (X_1, X_2, X_3)$  is the coordinate and  $I$  is the light intensity. Here the coordinate system is defined in the liquid resin, and we assume the same coordinate system should be applied to the as-reacted reference configuration which will be defined in the subsequent section (Fig. 1 and Fig. 2). In other words, we obtain the profile of DoC in the reference configuration from Eq. 1. As shown by the model, the DoC of cross-linked network is dependent on the light intensity and the reaction time. For photo field, since in 3D/4D printing light is irradiated unidirectionally, we will use a 1D photo-chemical field to describe the chemical reaction due to photopolymerization [11, 16, 42]. The distribution of light intensity inside the network can be determined through the Beer-Lambert law,

$$\frac{\partial I(\mathbf{X}, t)}{\partial X_3} = -\mu I(\mathbf{X}, t), \quad (2)$$

where  $\mu$  is the attenuation coefficient, and  $X_3$  is the coordinate along the light path

(Fig. 1). As shown by Eq. 2, when light is irradiated from one side (which is typical in 3D printing), a layer of liquid resin is exposed to irradiation from one side, the material points directly exposed to light will be under high intensity. The light intensity gradually attenuates in the material according to Eq. 2, and material points on the other side will be under low intensity.

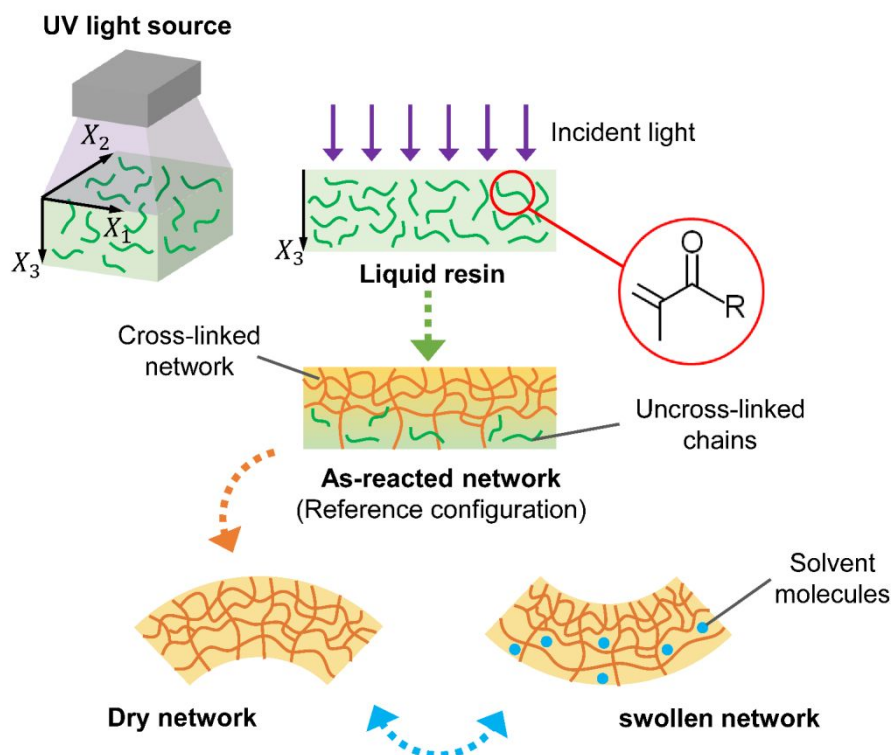


**Figure 1.** Schematic figure of the crosslink reaction and the desolvation/swelling process.

## 2.2. Kinematics and balance laws

After photo-crosslinking, although the partially cross-linked network always appears to be in a solid state, there may exist many uncross-linked monomer chains inside the network[44]. As shown in Fig.2, we assume that in the as-reacted configuration, there is no stress in the network [33]. It should be noted that stress could be developed later due to mechanical deformation events, such as non-uniform swelling.

Following the classical finite deformation theory[45], the material point denoted by  $\mathbf{X}$  in the reference configuration is moved to point  $\mathbf{x}$  in the current configuration, through the one-by-one mapping  $\mathbf{x}=\chi(\mathbf{X}, t)$ . The deformation gradient and the velocity are defined as,

$$\mathbf{F} = \nabla \chi, \mathbf{v} = \dot{\chi}. \quad (3)$$

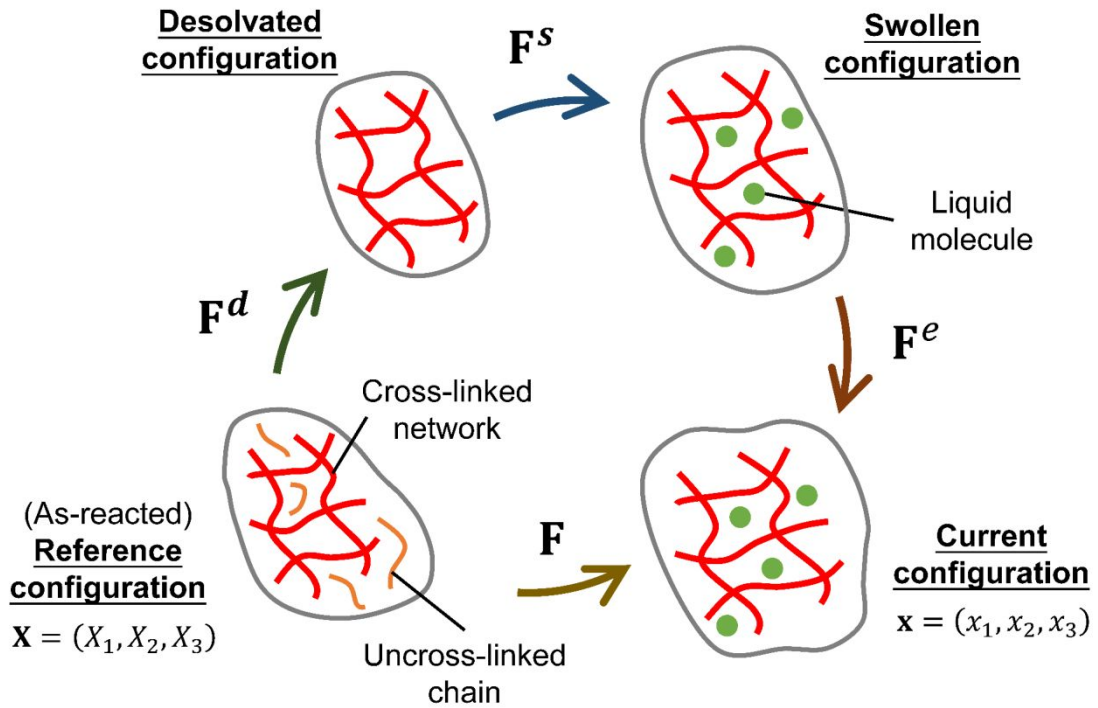


**Figure2.** Multiplicative decomposition of the deformation gradient.

As schematically shown in Fig. 2, the deformation gradient can be decomposed as,

$$\mathbf{F} = \mathbf{F}^e \mathbf{F}^s \mathbf{F}^d, \quad (4)$$

where  $\mathbf{F}^d$  is the desolvation deformation gradient,  $\mathbf{F}^s$  is the swelling deformation gradient and  $\mathbf{F}^e$  is the elastic deformation gradient. Here we assume the network deforms isotropically during desolvation and swelling. The desolvation deformation gradient has the form  $\mathbf{F}^d = \lambda^d \mathbf{I}$ , where  $\lambda^d$  is the desolvation stretch and  $\mathbf{I}$  is the unit tensor.

The swelling deformation gradient has the form  $\mathbf{F}^s = \lambda^s \mathbf{I}$ , where  $\lambda^s$  is the swelling stretch. Because the desolvation of a partially cross-linked network is irreversible (as discussed below), the desolvation deformation gradient  $\mathbf{F}^d$  will be a constant value at each material point and is a function of DoC, while the swelling deformation gradient  $\mathbf{F}^s$  and the elastic deformation gradient  $\mathbf{F}^e$  are dependent on the subsequent swelling conditions in the network. Due to non-uniform reaction in the network, the desolvation deformation gradient  $\mathbf{F}^d$  has different values at different material points. It remains to be constant once the chemical reaction is complete and thus is treated as a material point constant during swelling and desolvation. It should be noted, in this model we neglect the reaction-induced shrinkage deformation, which is intrinsic in photo-cross-linked polymers[42]. For real applications, most solvent responsive structures are cured under the confinement of molds, and the network is not allowed to shrink freely during reaction. This process significantly reduces the effect of reaction-induced shrinkage on subsequent deformations[46]. Now we define  $J = \det \mathbf{F}$ ,  $J^e = \det \mathbf{F}^e$ ,  $J^s = \det \mathbf{F}^s$ ,  $J^d = \det \mathbf{F}^d$  and the following relations hold,

$$J = J^e J^s J^d, J^d = (\lambda^d)^3, J^s = (\lambda^s)^3. \quad (5)$$

The partially photo-cross-linked network is composed by the network and the free uncrosslinked monomer chains. After desolvation, the free monomer chains will be cleaned away from the network. Here, we assume that once the free monomer chains are removed from the network, they cannot be bring back. The shrinkage of the network should be proportional to the volume of the free monomer chains. As a result, the desolvation stretch is expressed as,

$$\left(\lambda^d\right)^3 = 1 - \nu N^m c_0^m, \quad (6)$$

where  $\nu$  is the mole volume of a unit segment on the monomer chain,  $N^m$  is the equivalent length of the monomer chain, and  $c_0^m$  is the concentration of uncross-linked monomer chains right after photopolymerization. It should be noted,  $N^m$  indicates the number of unit segments on a single chain and it is a dimensionless value.  $c_0^m$  is related to the DoC as  $c_0^m = C_0(1-p)$ , where  $C_0$  is the concentration of monomer chains in the unreacted liquid resin.

The desolvated network without uncrosslinked monomers could be swollen by penetrating liquids. The swelling stretch is related to the concentrations of the fluid species,

$$\left(\lambda^s\right)^3 = \frac{1 + \nu c_R^s - \nu N^m c_0^m}{1 - \nu N^m c_0^m}, \quad (7)$$

where  $c_R^s$  is the concentration of the solvents measured in the reference configuration, and  $1 - \nu N^m c_0^m$  is the volume of the network after desolvation. Following Floy's assumption, we assume the mole volume of the solvent molecule is  $\nu$ , which is equal to the mole volume of a unit segment on the monomer chain[47].

The left Cauchy-Green tensor and the right Cauchy-Green tensor are defined as,

$$\mathbf{B} = \mathbf{F}\mathbf{F}^T, \mathbf{C} = \mathbf{F}^T\mathbf{F}. \quad (8)$$

In addition,

$$\mathbf{C}^e = \mathbf{F}^{eT}\mathbf{F}^e. \quad (9)$$

Next we examine the balance laws of the system. The first Piola-Kirchhoff stress is defined as,

$$\mathbf{S} = J\boldsymbol{\sigma}\mathbf{F}^{-T}, \quad (10)$$

where the Cauchy stress  $\boldsymbol{\sigma}$  is correlated to the surface traction  $\mathbf{t}$  as,

$$\boldsymbol{\sigma}\mathbf{N} = \mathbf{t}. \quad (11)$$

Here  $\mathbf{N}$  is the unit normal vector of an arbitrary surface in the current configuration.

The balance equations of force and moment in the reference configuration can be written as,

$$Div\mathbf{S} + \mathbf{b}_R = \mathbf{0}, \quad (12A)$$

$$\mathbf{S}\mathbf{F}^T = \mathbf{F}^T\mathbf{S}, \quad (12B)$$

where  $\mathbf{b}_R$  is the body force measured in the reference configuration.

The balance of the liquid solvents is described by the Fick's law[48],

$$\mathfrak{E}_R = -Div\mathbf{j}_R^s, \quad (13)$$

where  $\mathfrak{E}_R$  is the rate of the solvent concentration in the reference configuration,  $\mathbf{j}_R^s$  is the fluid flux measured in the reference configuration. It should be noted, Fick's law is required for the derivation of thermodynamic restrictions, but only the equilibrium process will be considered in the subsequent simulations and analysis.

### 2.3. Free energy function and thermodynamic restrictions

The free energy function of the thermodynamic system measured in the reference configuration can be written in a separable form [21, 25, 33],

$$\psi_R(\mathbf{C}^e, c_R^s) = \mu_0^s c_R^s + \psi_M(\mathbf{C}^e, c_R^s) + \psi_S(c_R^s), \quad (14)$$

Here  $\mu_0^s$  is the chemical potentials of the pure solvent measured in the reference configuration. The second term in Eq. 14 is the contribution from mechanical deformation, and the third term is the contribution due to the mixing of fluid species in the cross-linked network.

For the mechanical part in the free energy function, we adopt the compressible neo-Hookean model proposed by Chester et al[35],

$$\psi_M(\mathbf{C}^e, c_R^s) = \frac{1}{2}G(\text{tr}\mathbf{C} - 3 - 2\ln J) + J^s J^d \frac{1}{2}K(\ln J^e)^2, \quad (15)$$

where  $G$  and  $K$  are the shear modulus and the bulk modulus, respectively. Here we only consider the elastic deformation, because for long-time period the viscoelasticity of polymer network is not obvious compared with the migration of solvents [49]. The shear modulus  $G$  is correlated to the DoC of the network as [11, 42],

$$G = G_c \exp\left(b(p - p_{gel})\right) + G_d, \quad (16)$$

where  $p_{gel}$  is the DoC at the gelation point, and the remaining parameters are some constants. The bulk modulus  $K$  is always chosen to be sufficiently large to imitate the incompressibility behavior[35, 50] (e.g. 100 times than the shear modulus).

The chemical mixing part in the free energy function can be determined according to the Flory lattice theory as[17, 47],

$$\psi_S(c_R^s) = kT(c_R^s \ln \frac{vc_R^s}{1 + vc_R^s - vN^m c_0^m} + \chi_{ps} \frac{c_R^s(1 - vN^m c_0^m)}{1 + vc_R^s - vN^m c_0^m}). \quad (17)$$

Here  $\chi_{ps}$  is the interaction parameter between the network and the solvent, which is dependent on both the type of the solution and the DoC of the network[51, 52],

$$\chi_{ps} = \chi_{ps}^0 + \alpha p, \quad (18)$$

where  $\chi_{ps}^0$  and  $\alpha$  are two constant parameters.

Considering the materials occupies the region  $V$  in the reference configuration, the second law of thermodynamics can be described by[45],

$$\int_V \mathbf{t} \cdot \mathbf{n} dV - \int_{\partial V} \mathbf{t} \mathbf{v} dS - \int_V \mathbf{b}_R \mathbf{v} dV + \int_{\partial V} \mu_0^s \mathbf{j}_R^s \mathbf{N} dS \leq 0, \quad (19)$$

where  $\partial V$  is the boundary of the region. Utilizing Gauss's theorem, Eq. 19 can be

transformed to,

$$\int_V (\mathbf{S} : \mathbf{F} - \mu^s \text{Div} \mathbf{j}_R^s - \mathbf{j}_R^s \nabla \mu^s) dV + \int_V (\text{Div} \mathbf{S} + \mathbf{b}_R) \mathbf{v} dV \leq 0. \quad (20)$$

Inserting Eq. 12 and Eq. 13 into Eq. 20 and utilizing the Coleman-Noll procedure[53],

we obtain the expression of the Cauchy stress[26],

$$\boldsymbol{\sigma} = J^{-1} \left( 2\mathbf{F}^e \frac{\partial \psi}{\partial \mathbf{C}^e} \mathbf{F}^{eT} \right) = J^{-1} [G(\mathbf{B} - \mathbf{I}) + J^s J^d K \ln J^e \mathbf{I}], \quad (21)$$

and the expressions of the chemical potential,

$$\begin{aligned} \mu^s = \frac{\partial \psi}{\partial c_R^s} - \frac{\nu}{3} J^e \text{tr} \boldsymbol{\sigma} = \mu_0^s + kT \left[ \ln \frac{\nu c_R^s}{1 + \nu c_R^s - \nu N^m c_0^m} + \frac{1 - \nu N^m c_0^m}{1 + \nu c_R^s - \nu N^m c_0^m} \right. \\ \left. + \chi_{ps} \frac{(1 - \nu N^m c_0^m)^2}{(1 + \nu c_R^s - \nu N^m c_0^m)^2} \right] + \frac{1}{2} K \nu (\ln J^e)^2 - \nu K \ln J^e \end{aligned} \quad (22)$$

### 3. Results

#### 3.1. Finite element implementation of the model

The above finite deformation theory was implemented in the commercial finite element analysis (FEA) software ABAQUS (Dassault Systems, Waltham, MA, USA) for simulations. In this paper, we are most interested in the equilibrium response of the partially photo-cross-linked network upon desolvation and swelling, and the diffusion process was not included in the simulations. We used the user subroutine UHYPER in ABAQUS to describe the mechanical behaviors of the network, and the free energy function in Eq. 14 and its derivatives were imported to the subroutine. Normally we used two steps in the simulations. In the first step, the kinetics in Eq. 1 and Eq. 2 were solved to obtain the distribution of the DoC inside the material. If the attenuation coefficient is constant inside the material, these two equations can be simplified to

$$p = 1 - \exp(-K_r I_0 \exp(-\mu X_3) t), \quad (23)$$

where  $X_3$  is the distance along the light path, and  $I_0$  is the incident light intensity that varies as a function of  $X_1$  and  $X_2$ .

In the second step, the concentration of solvent was decided according to the swelling condition, and the deformation of the whole structure could be obtained. Specifically, after the desolvation process there is no fluid species inside the network, and the concentration of the solvent should be  $c_R^s = 0$ . However, in order to avoid numerical singularity in the total free energy[33], the concentration of the solvent was set to a relatively small value (0.001) in the simulations. In contrast, if the desolvated network is allowed to be free swollen in the solvent, the concentration of the solvent inside the network was decided through the stress-free condition  $\sigma = 0$ , together with the requirement that the chemical potential of the system should be equal to the chemical potential of pure solvent  $\mu^s = \mu_0^s$ . This calculation typically involves implicit iterations in the software.

### 3.2. Simulations of desolvation induced shape change

In this subsection, we show the efficiency of the theory in the simulation of desolvation induced shape changes in partially photo-cross-linked polymers. When a polymer film is photo-crosslinked by irradiating light from one side, the crosslink density across the thickness of the film is nonuniform. The side directly exposed to light is highly crosslinked, while the other side is loosely crosslinked. If the film undergoes desolvation, the uncrosslinked chains inside the film will be washed away and the film bends towards the loosely cross-linked side. This mechanism has been used to fabricate complex 3D structures that can be derived by flat polymer films [11, 12]. When the 3D

structure is immersed in good solvents, the deformation can be recovered through swelling. Because relatively hard polymers are always utilized, the swelling ratio would not be large enough to drive the film to deform towards the opposite direction (Fig. 3D).

### 3.2.1. Parameters identification

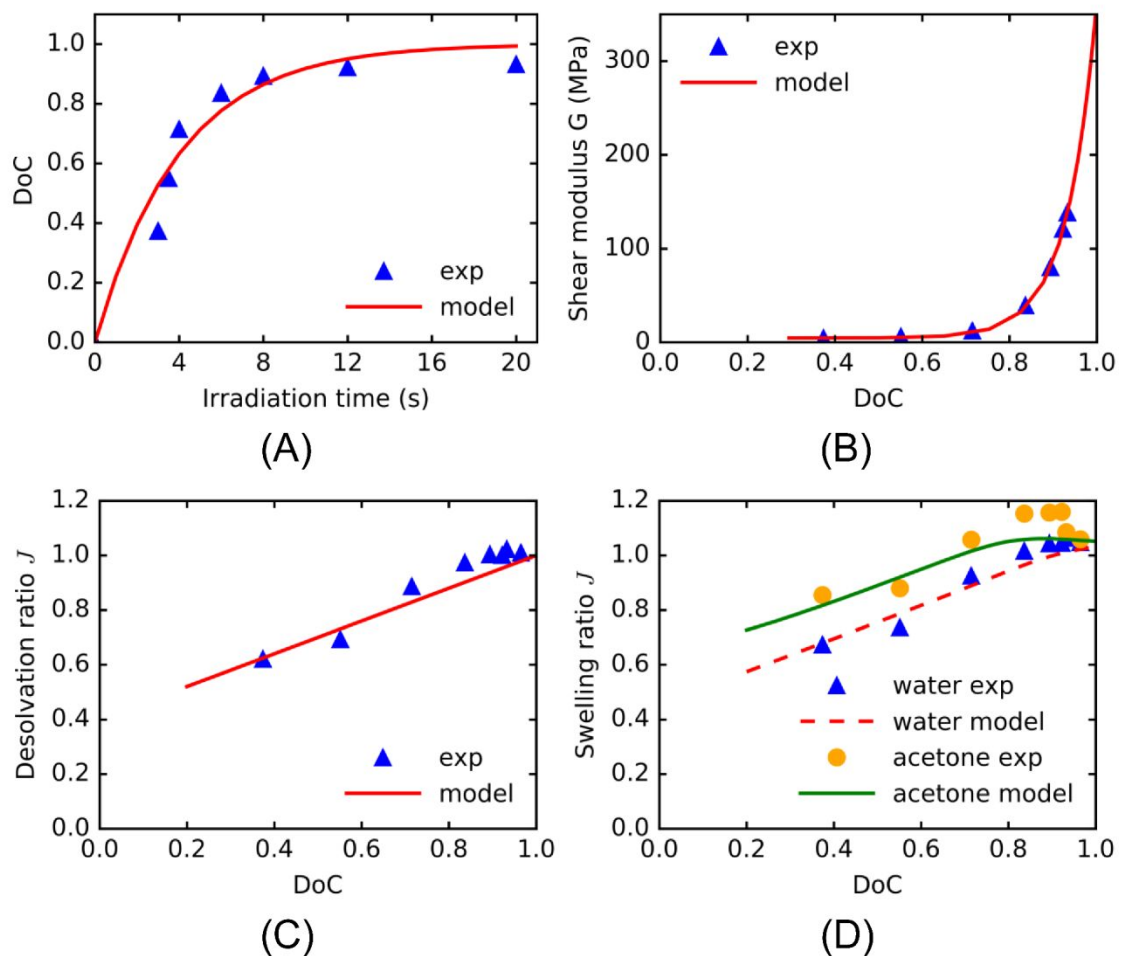


**Figure 3.** (A) The DoC as a function of irradiation time. (B) The shear modulus  $G$  as a function of the DoC. (C) The desolvation ratio as a function of the DoC. (D) The swelling ratio in water and acetone as a function of the DoC. (The experiment results are from Zhao et al[11])

The parameters in the model were obtained by fitting the experimental results of photo-crosslinked PEGDA in our previous works[11]. In these experiments, ultra-thin polymer samples without adding photoabsorbers were irradiated for different times to

obtain uniformly crosslinked networks with different crosslink densities. The swelling and desolvation behaviors of the samples were also uniform. The fundamental material properties are summarized in Fig.3, and the corresponding model parameters are listed in Table 1. When the liquid resin was exposed to light irradiation, the DoC and the shear modulus of the cross-linked network increased with time (Fig. 3A-B). The reaction coefficient  $K$  could be obtained by fitting Fig. 3A, and the attenuation parameter was obtained from the evolution of curing depth in our previous work[11]. The initial concentration of monomers  $C_0$  was calculated from the formula of liquid resin. We also calculated the constant parameters  $G_c$ ,  $b$  and  $G_d$  in Eq. 16 by fitting Fig. 3B. The desolvation ratio and the swelling ratio are defined as the total volume ratio  $J$  after desolvation and swelling, respectively. The desolvation ratio, which is related to the amount of residual free monomer chains inside the network, decreased with the growing of DoC (Fig. 3C). According to the assumptions of Eq. 6 and Eq. 7, the mole volume of the monomer segment was set to the typical value in swelling problems[33, 35], and the effective chain length  $N^m$  could be obtained by fitting Fig. 3C. There was no desolvation-induced volume shrinkage in the fully cross-linked network (The DoC equals to 1). Fig 3D shows the free-swelling ratio of the dry network in different types of solvents. Large swelling-induced expansion could be obtained by immersing the loosely crosslinked network in good solvents (for example acetone). The swelling ratio of the fully-crosslinked network was slightly higher than 1, which indicates it still retained some ability to swell. Finally the swelling parameters in Eq. 18 were acquired by simulating and fitting the experiment results in Fig. 3D.

Table 1. Model parameters for section 3.2

Parameters	Value	Description
$K_r (mW^{-1}cm^2s^{-1})$	0.05	Reaction coefficient[11]
$\mu (mm^{-1})$	17	Attenuation coefficient[11]
$C_0 (mol L^{-1})$	4.44	Initial monomer concentration
$N^m$	0.00075	Equivalent length of the chains
$v (L mol^{-1})$	180	Mole volume of the solvent[35]
$G_c (MPa)$	0.0015	Fitting parameter
$b$	14.75	Fitting parameter
$p_{gel}$	0.16	DoC at the gelation point[11, 42]
$G_d$	4.5	Fitting parameter
$\chi_{ps}^0$	1.1(acetone)	Fitting parameter
	2(water)	
$\alpha$	0.15	Fitting parameter

### 3.2.2. Desolvation induced bending of differentially cross-linked strips

As the first example, we show the simulation results of a differentially cross-linked strip upon desolvation and swelling. Here a strip with a thickness of 0.2mm was investigated, and the incident light intensity was fixed to  $5mWcm^{-2}$ . Because of the nonuniform crosslink density across the thickness, the strip bent towards the loosely cross-linked side upon desolvation, and it recovered to the flat shape upon swelling in acetone (Fig. 4A-B). As shown in Fig. 4A, internal stress arises from incompatibility after all the solvents and un-crosslinked chains are removed from the network. For short irradiation times, the side directly exposed to light was fully cross-linked, while the

other side was loosely cross-linked because the light intensity was attenuated on this side (for example the profile of DoC after 10s irradiation in Fig. 4D). As a result, there were a large amount of residual chains on the loosely cross-linked side, which caused large shrinkage and significant bending curvature upon desolvation. For long irradiation times, although the side opposite to the light source was still under low intensity, there was enough time for the network to be fully cross-linked, and the profile of DoC became more uniform across the thickness (for example the profile of DoC after 160s irradiation in Fig. 4D). In this case, the bending curvature after desolvation would decrease at the same time.

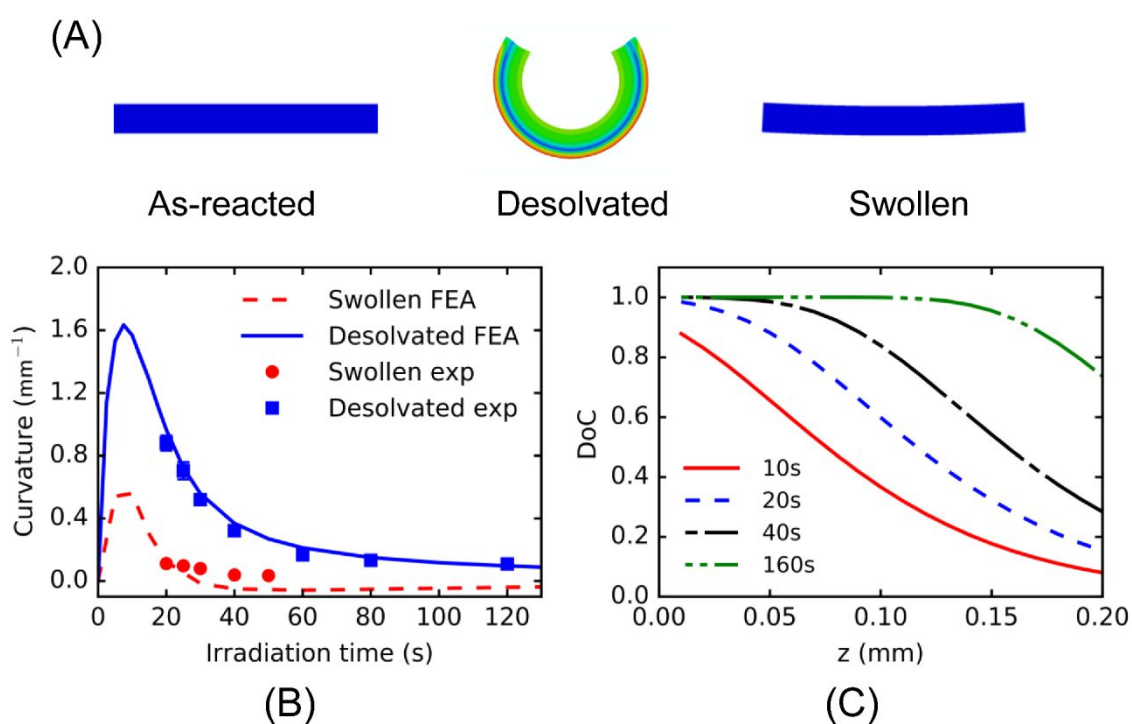


**Figure 4.** (A) The schematic figure of desolvation induced bending and swelling induced shape recovery. (B) The bending curvature as a function of the photopolymerization irradiation time. (C) The DoC profiles across the thickness of different photopolymerization irradiation times. (The experiment results are from Zhao et al[11])

Based on the theoretical framework, we were able to investigate several

predominant factors that can influence the desolvation induced bending deformation. Here the irradiation times of the strips were fixed to 20s. As shown in Fig. 5A-B ( $\mu=17\text{mm}^{-1}$ , thickness= $0.2\text{mm}$ ), a lower incident light intensity resulted in a higher bending curvature upon desolvation, because a much nonuniform profile of DoC was created. But under extremely low intensity, even the side directly exposed to light could not be fully crosslinked, and the final bending curvature was reduced. The influence of the attenuation ability is shown in Fig. 5C-D ( $I_0=5\text{mWcm}^{-2}$ , thickness= $0.2\text{mm}$ ). Increasing the attenuation coefficient always resulted in more loosely crosslinked network at the side opposite to the light source, while the side directly exposed to light could always be fully cross-linked. As a result, the bending curvature monotonically increased with the attenuation coefficient. As shown in Fig. 5E-F ( $I_0=5\text{mWcm}^{-2}$ ,  $\mu=20\text{mm}^{-1}$ ), moderately increasing the total thickness of the strip resulted in higher bending curvature, which came from the higher gradient of DoC across the thickness. But if the thickness was too large, liquid polymers at the side opposite to the light source could not be cross-linked (for example the DoC profile of  $0.3\text{mm}$  in Fig. 5F), and the bending curvature would not further increase any more.

### 3.2.3. Desolvation induced shape changing with DLP

Inspired by the above discussion, if the irradiation condition along the strip could be manipulated, the desolvation induced bending curvature would also vary following specific patterns. This can be achieved by controlling the distribution of light intensity during photopolymerization, which can be easily implemented by irradiating grayscale light patterns to the liquid resin[14]. Some special structures realized by this method

are shown in Fig. 6 (irradiation time=20s,  $\mu=17\text{mm}^{-1}$ , thickness=0.2mm). For example, if a light pattern with the distribution of intensity following the top of Fig. 6A was utilized to cure the strip, the two ends crosslinked under low intensity displayed higher bending curvature upon desolvation, while the center part crosslinked under high intensity displayed relatively small curvature. We could also control the distribution of light intensity on both sides of the strip. As shown in Fig. 6C-D, the strip would be able to bend towards two different directions, and complex shapes were created upon desolvation of the strip. As shown by the inset, the negative light intensity in Fig. 6C-D indicates the irradiation of the light pattern from an opposite side of the strip.

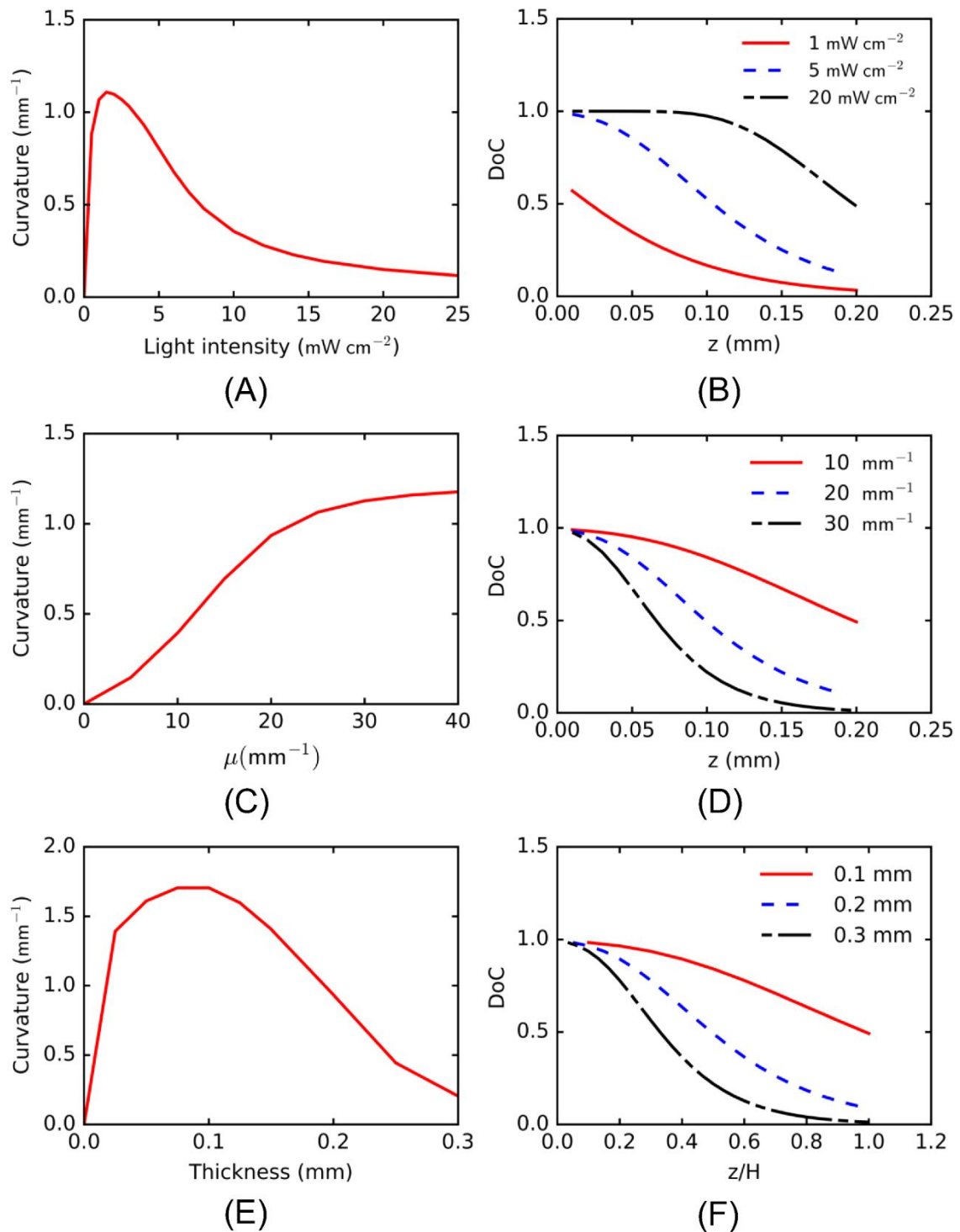


**Figure 5.** (A) The desolvation induced bending curvature as a function of the incident light intensity. (B) The DoC profiles under different incident light intensities. (C) The desolvation induced bending curvature as a function of the attenuation coefficient. (D) The DoC profiles for different attenuation coefficients. (E) The desolvation induced bending curvature as a function of the film thickness. (F) The DoC profiles of strips with different total thicknesses.

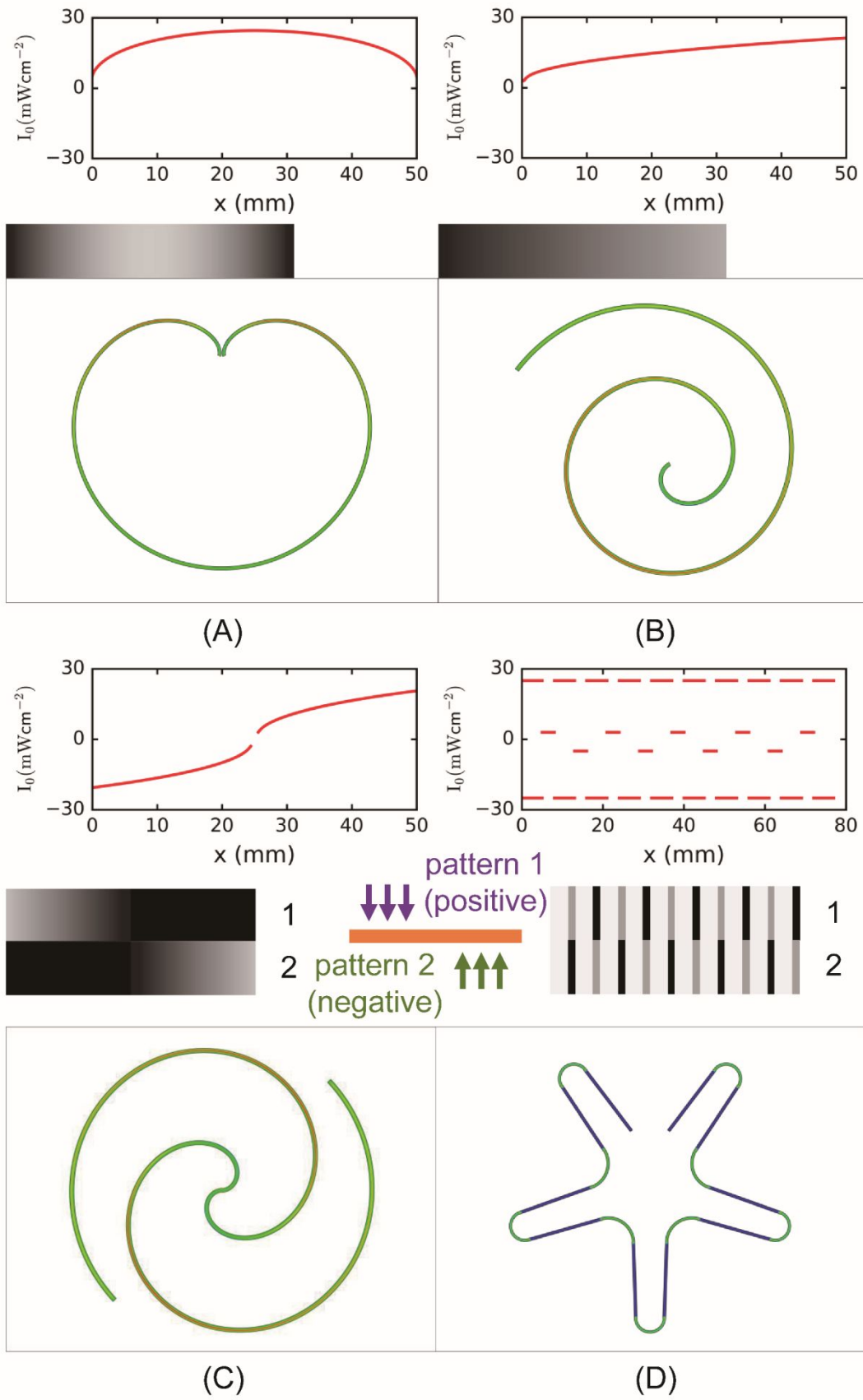


**Figure 6.** (A) The desolvation induced bending towards a heart. (B) The desolvation induced bending towards a helix. (C) The desolvation induced bending towards a double helix. (D) The desolvation induced bending towards a star. (The distributions of light intensity on the strips and the corresponding grayscale patterns are listed on the top of each figure. Here the length is not scaled to the actual structure on the bottom.)

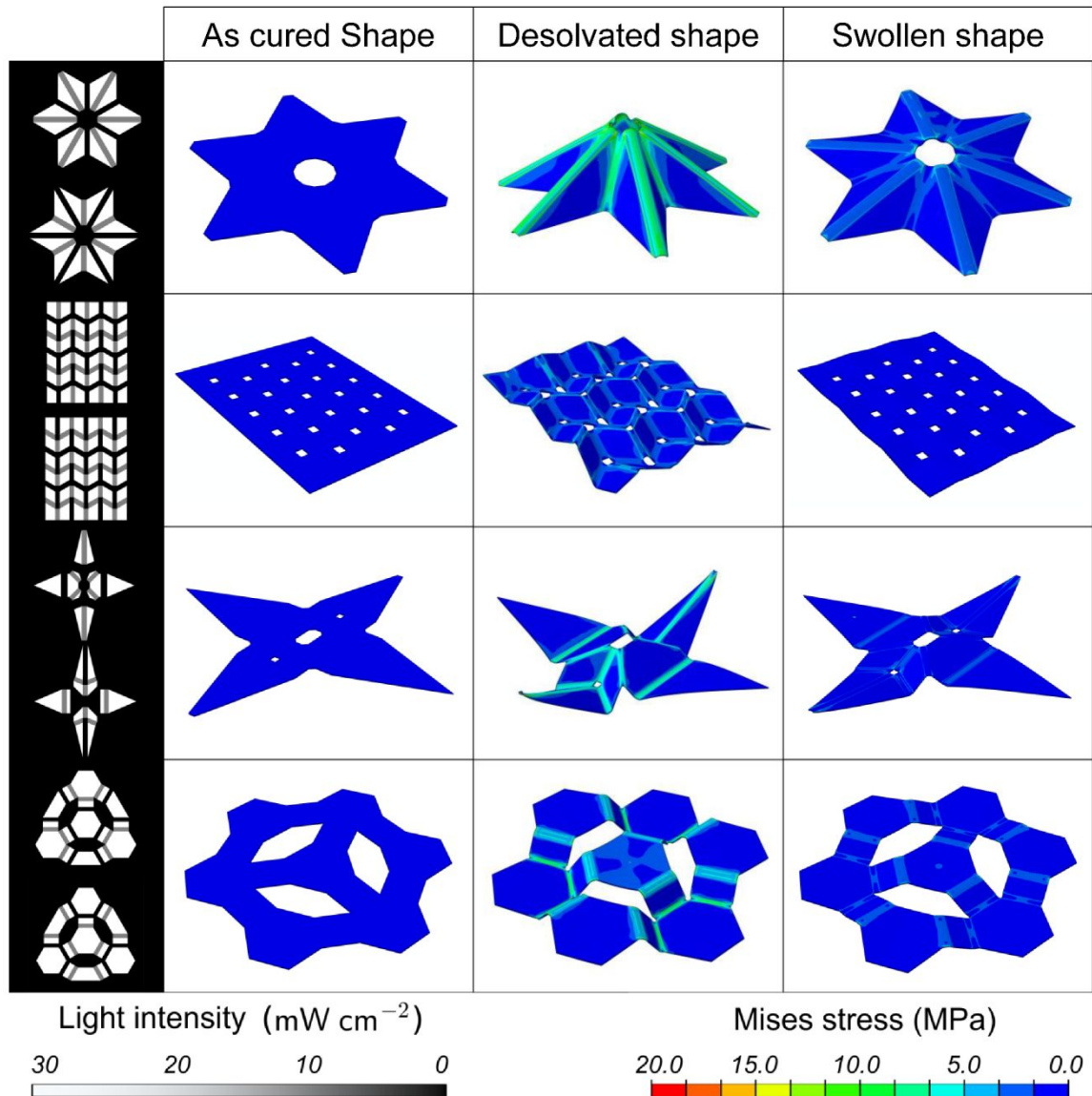


**Figure 7.** The desolvation induced origami and shape recovery of different structures. (The distributions of light intensity on the strips are listed on the left of each structure, and the simulation parameters were set to the actual conditions in the work of Zhao et al[11])

The theoretical framework could also be used to predict the desolvation induced deformation of structures with more complex shapes. Previously, Zhao et al[11]

showed the desolvation induced origami of differentially photo-cross-linked polymers for 4D printing. By using specific planner light patterns to cure the polymer sheet, 3D origami shapes such as the Miura-ori structure and the origami crane could be created upon desolvation. The origami structure recovered to the flat shape once the structure was immersed in acetone. Similar to the concept in Fig. 6, the folding of the planner polymer sheet was realized by imposing low light intensity at the folding creases while high intensity at the flat panels. The simulation results of different types of origami structures are shown in Fig. 7, where the simulation parameters were set to the values in the experiment works of Zhao et al[11]. Both the desolvation induced origami and the swelling induced shape recovery could be predicted well by the theoretical framework. Because of the strain mismatch during desolvation, the stress was higher at the folding creases of the structures.

### 3.3. Simulations of swelling induced shape change

Here, we show the simulation results of the swelling induced shape change in partially photo-crosslinked polymers presented in the recent work of Huang et al[16] for 4D printing. Following the same procedure in section 3.1, the model parameters were obtained by fitting the experiment results in Huang et al[16] (Fig. 8), and the corresponding values are listed in Table 2. The experiments were also implemented by using uniformly crosslinked samples with different crosslink densities. Different from the conditions in section 3.2, Huang et al[16] utilized soft hydrogels which undergoes large volume expansion upon swelling. As shown in Fig. 8D, the swelling ratio of the loosely cross-linked network was much higher than that of the fully cross-linked

network, and the swelling ratio was also significantly higher than that of the hard polymers in Fig. 3D. Upon desolvation, with the shrinkage of the loosely cross-linked network (Fig. 8C), the polymer sheet deforms to the first shape. When the desolvated structure is immersed in good solvent, significant volume expansion occurs in the loosely cross-linked network, and the polymer film deforms towards the opposite direction. From the theoretical point of view, this phenomenon is a result of the relatively small modulus ( $G$  and  $K$ ) and the small interaction parameter  $\chi_{ps}$ .

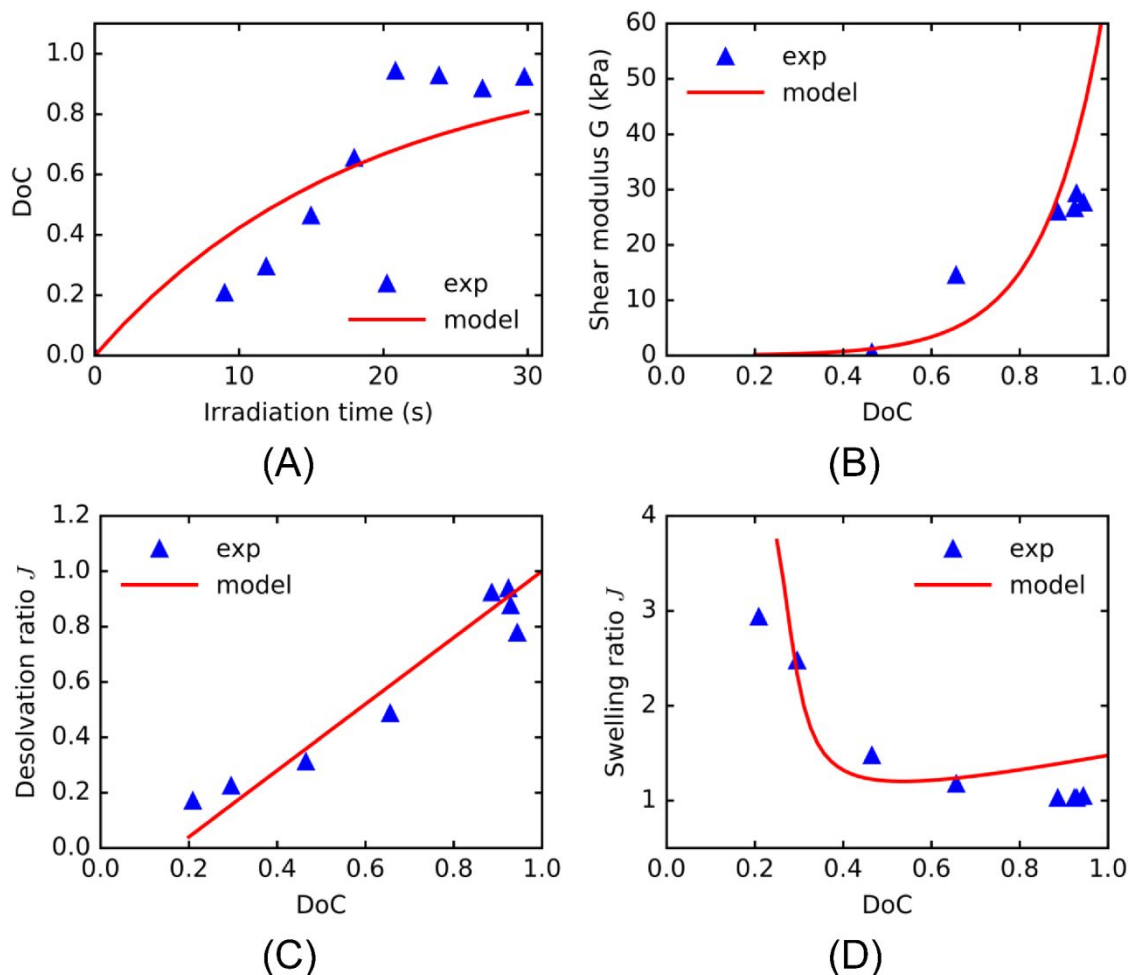


**Figure 8.** (A) The DoC as a function of irradiation time. (B) The shear modulus  $G$  as a function of the DoC. (C) The desolvation ratio as a function of the DoC. (D) The swelling ratio as a function of the DoC. (The experiment results are from Huang et al[16])

Table 2. Model parameters for section 3.3

Parameters	Value	Description
$K_r (mW^{-1}cm^2s^{-1})$	0.011	Reaction coefficient
$\mu (mm^{-1})$	0	Attenuation coefficient
$C_0 (mol L^{-1})$	5	Initial monomer concentration
$N^m$	0.0013	Length of the chains
$v (Lmol^{-1})$	180	Mole volume of the solvent
$G_c (MPa)$	0.0005	Fitting parameter
$b$	7.5	Fitting parameter
$p_{gel}$	0.2	DoC at the gelation point
$G_d$	0	Fitting parameter
$\chi_{ps}^0$	0.33	Fitting parameter
$\alpha$	0.65	Fitting parameter

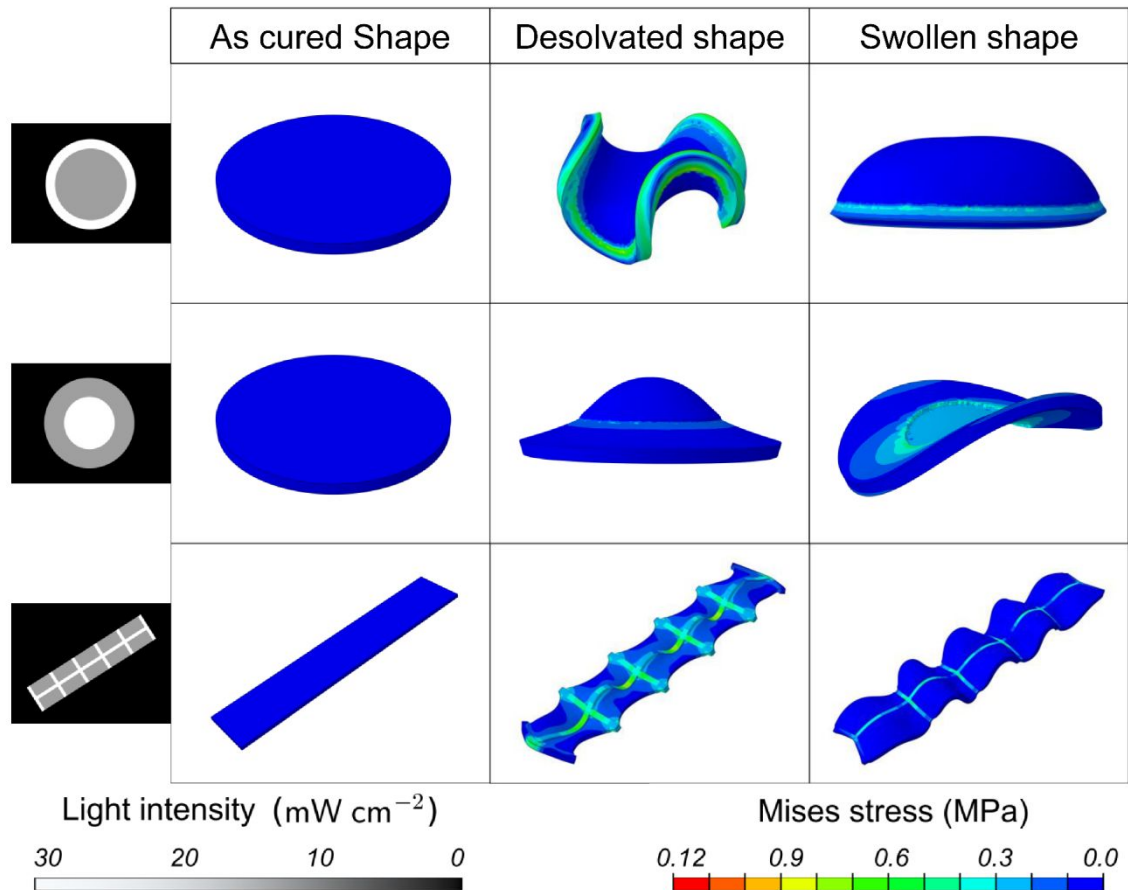


**Figure 9.** The swelling induced shape change of different structures.

The simulation results of some swelling induced shape changing structures are shown in Fig. 9. Consistent with the experiment conditions of Huang et al[16], here we assumed there was no light attenuation across the thickness of the film, and the crosslink density only varies in the planner plane according to the incident light patterns. Different from the results in Fig. 7, each structure had two deformed shapes upon desolvation and swelling, respectively. For example, if the circular plate was loosely cross-linked at the center while fully cross-linked at the edge, it deformed to the saddle shape upon desolvation. If the saddle was immersed in good solvent, it deformed conversely to the dome shape.

#### 4. Conclusions

In this paper, we proposed a finite deformation theory to describe the desolvation and swelling process of partially photo-cross-linked polymers. Starting from the analysis of the underlying photopolymerization kinetics, the crosslink density of the polymer network was correlated to the irradiation conditions, for example the irradiation time and the incident light intensity. We chose the pure polymer network without residual free chains as the reference configuration of the thermodynamic system, while the as-reacted network was treated as a free swollen configuration. By using this specific choice of configuration, the desolvation and swelling process were transformed to the behaviors of the differentially cross-linked network in a binary mixture system. The theory was implemented in the FEA software to simulate the behaviors of different types of partially photo-cross-linked materials. We showed the efficiency of the theory in the simulations under two specific conditions. Both the desolvation induced origami and the swelling induced shape change could be well predicted by the theoretical framework. The theory and the simulation method can be utilized in the future design and analysis of different types of solvent responsive structures.

### **Acknowledgement**

HJQ acknowledge the support of an AFOSR grant (FA9550-16-1-0169; Dr. B.-L. “Les” Lee, Program Manager) and gift funds from HP, Inc and Northrop Grumman Corporation. ZZ and DF acknowledge a support from National Natural Science Foundation of China (11521202) and a support from National Materials Genome

Project of China (2016YFB0700600). ZZ acknowledges a support from China Scholarship Council (No. 201506010219).

## References

1. Lee, H., C.G. Xia, and N.X. Fang, *First jump of microgel; actuation speed enhancement by elastic instability*. *Soft Matter*, 2010. **6**(18): p. 4342-4345.
2. Jamal, M., et al., *Bio-Origami Hydrogel Scaffolds Composed of Photocrosslinked PEG Bilayers*. *Advanced Healthcare Materials*, 2013. **2**(8): p. 1142-1150.
3. Randall, C.L., E. Gultepe, and D.H. Gracias, *Self-folding devices and materials for biomedical applications*. *Trends in Biotechnology*, 2012. **30**(3): p. 138-146.
4. Fernandes, R. and D.H. Gracias, *Self-folding polymeric containers for encapsulation and delivery of drugs*. *Advanced Drug Delivery Reviews*, 2012. **64**(14): p. 1579-1589.
5. Zhang, H., et al., *Soft mechanical metamaterials with unusual swelling behavior and tunable stress-strain curves*. *Science Advances*, 2018. **4**(6).
6. Silverberg, J.L., et al., *Origami structures with a critical transition to bistability arising from hidden degrees of freedom*. *Nature Materials*, 2015. **14**(4): p. 389-393.
7. Kuang, X., et al., *Advances in 4D Printing: Materials and Applications*. *Advanced Functional Materials*, 2018: p. 1805290.
8. Mao, Y.Q., et al., *3D Printed Reversible Shape Changing Components with Stimuli Responsive Materials*. *Scientific Reports*, 2016. **6**.
9. Gladman, A.S., et al., *Biomimetic 4D printing*. *Nature Materials*, 2016. **15**(4): p. 413-+.
10. Raviv, D., et al., *Active Printed Materials for Complex Self-Evolving Deformations*. *Scientific Reports*, 2014. **4**.
11. Zhao, Z., et al., *Desolvation Induced Origami of Photocurable Polymers by Digit Light Processing*. *Macromol Rapid Commun*, 2017. **38**(13).

12. Jamal, M., A.M. Zarafshar, and D.H. Gracias, *Differentially photo-crosslinked polymers enable self-assembling microfluidics*. Nature Communications, 2011. **2**.
13. Guvendiren, M., S. Yang, and J.A. Burdick, *Swelling-Induced Surface Patterns in Hydrogels with Gradient Crosslinking Density*. Advanced Functional Materials, 2009. **19**(19): p. 3038-3045.
14. Wu, J., et al., *Reversible shape change structures by grayscale pattern 4D printing*. Multifunctional Materials, 2018. **1**(1): p. 015002.
15. Han, D., et al., *Micro 3D Printing of a Temperature-Responsive Hydrogel Using Projection Micro-Stereolithography*. Sci Rep, 2018. **8**(1): p. 1963.
16. Huang, L.M., et al., *Ultrafast Digital Printing toward 4D Shape Changing Materials*. Advanced Materials, 2017. **29**(7).
17. Rubinstein, M. and R.H. Colby, *Polymer physics*. Vol. 23. 2003: Oxford University Press New York.
18. Flory, P.J. and J. Rehner, *Statistical mechanics of cross-linked polymer networks I Rubberlike elasticity*. Journal of Chemical Physics, 1943. **11**(11): p. 512-520.
19. Flory, P.J. and J. Rehner, *Statistical mechanics of cross-linked polymer networks II Swelling*. Journal of Chemical Physics, 1943. **11**(11): p. 521-526.
20. Gibbs, J.W., *The scientific papers of J. Willard Gibbs*. Vol. 1. 1906: Longmans, Green and Company.
21. Flory, P.J., *Statistical Mechanics of Swelling of Network Structures*. Journal of Chemical Physics, 1950. **18**(1): p. 108-111.
22. Biot, M.A., *Nonlinear and Semilinear Rheology of Porous Solids*. Journal of

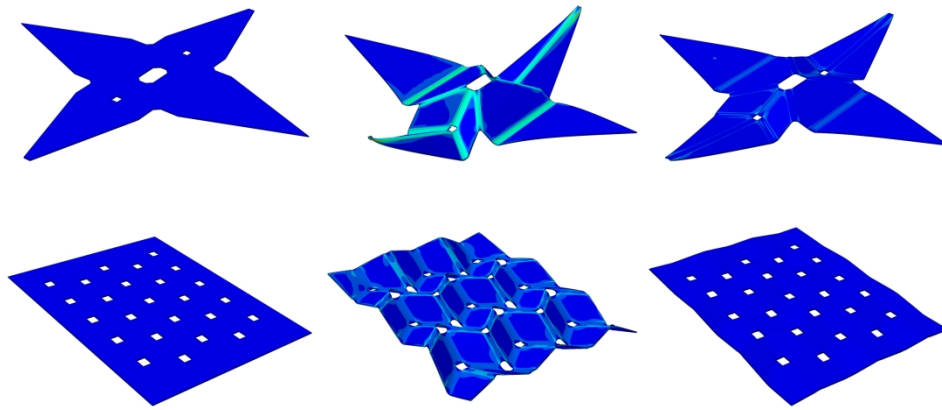
- Geophysical Research, 1973. **78**(23): p. 4924-4937.
23. Hong, W., et al., *A theory of coupled diffusion and large deformation in polymeric gels*. Journal of the Mechanics and Physics of Solids, 2008. **56**(5): p. 1779-1793.
24. Duda, F.P., A.C. Souza, and E. Fried, *A theory for species migration in a finitely strained solid with application to polymer network swelling*. Journal of the Mechanics and Physics of Solids, 2010. **58**(4): p. 515-529.
25. Chester, S.A. and L. Anand, *A coupled theory of fluid permeation and large deformations for elastomeric materials*. Journal of the Mechanics and Physics of Solids, 2010. **58**(11): p. 1879-1906.
26. Chester, S.A. and L. Anand, *A thermo-mechanically coupled theory for fluid permeation in elastomeric materials: Application to thermally responsive gels*. Journal of the Mechanics and Physics of Solids, 2011. **59**(10): p. 1978-2006.
27. Cai, S.Q. and Z.G. Suo, *Mechanics and chemical thermodynamics of phase transition in temperature-sensitive hydrogels*. Journal of the Mechanics and Physics of Solids, 2011. **59**(11): p. 2259-2278.
28. Marcombe, R., et al., *A theory of constrained swelling of a pH-sensitive hydrogel*. Soft Matter, 2010. **6**(4): p. 784-793.
29. Hui, C.Y. and R. Long, *A constitutive model for the large deformation of a self-healing gel*. Soft Matter, 2012. **8**(31): p. 8209-8216.
30. Zhao, X.H., *A theory for large deformation and damage of interpenetrating polymer networks*. Journal of the Mechanics and Physics of Solids, 2012. **60**(2): p. 319-332.
31. Deghany, M., et al., *A thermodynamically-consistent large deformation theory*

- coupling photochemical reaction and electrochemistry for light-responsive gels*. Journal of the Mechanics and Physics of Solids, 2018. **116**: p. 239-266.
32. Long, R., H.J. Qi, and M.L. Dunn, *Thermodynamics and mechanics of photochemically reacting polymers*. Journal of the Mechanics and Physics of Solids, 2013. **61**(11): p. 2212-2239.
33. Hong, W., Z.S. Liu, and Z.G. Suo, *Inhomogeneous swelling of a gel in equilibrium with a solvent and mechanical load*. International Journal of Solids and Structures, 2009. **46**(17): p. 3282-3289.
34. Duan, Z., et al., *Simulation of the Transient Behavior of Gels Based on an Analogy Between Diffusion and Heat Transfer*. Journal of Applied Mechanics-Transactions of the Asme, 2013. **80**(4).
35. Chester, S.A., C.V. Di Leo, and L. Anand, *A finite element implementation of a coupled diffusion-deformation theory for elastomeric gels*. International Journal of Solids and Structures, 2015. **52**: p. 1-18.
36. Bouklas, N., C.M. Landis, and R. Huang, *A nonlinear, transient finite element method for coupled solvent diffusion and large deformation of hydrogels*. Journal of the Mechanics and Physics of Solids, 2015. **79**: p. 21-43.
37. Guo, W., M.E. Li, and J.X. Zhou, *Modeling programmable deformation of self-folding all-polymer structures with temperature-sensitive hydrogels*. Smart Materials and Structures, 2013. **22**(11).
38. Yagci, Y., S. Jockusch, and N.J. Turro, *Photoinitiated Polymerization: Advances, Challenges, and Opportunities*. Macromolecules, 2010. **43**(15): p. 6245-6260.

39. Goodner, M.D. and C.N. Bowman, *Development of a comprehensive free radical photopolymerization model incorporating heat and mass transfer effects in thick films*. Chemical Engineering Science, 2002. **57**(5): p. 887-900.
40. Bauhofer, A.A., et al., *Harnessing Photochemical Shrinkage in Direct Laser Writing for Shape Morphing of Polymer Sheets*. Adv Mater, 2017.
41. Wu, Z.G., N. Bouklas, and R. Huang, *Swell-induced surface instability of hydrogel layers with material properties varying in thickness direction*. International Journal of Solids and Structures, 2013. **50**(3-4): p. 578-587.
42. Wu, J., et al., *Evolution of material properties during free radical photopolymerization*. Journal of the Mechanics and Physics of Solids, 2018. **112**: p. 25-49.
43. Cabral, J.T., et al., *Frontal photopolymerization for microfluidic applications*. Langmuir, 2004. **20**(23): p. 10020-10029.
44. Hennessy, M.G., et al., *Monomer diffusion into static and evolving polymer networks during frontal photopolymerisation*. Soft Matter, 2017.
45. Gurtin, M.E., E. Fried, and L. Anand, *The mechanics and thermodynamics of continua*. 2010: Cambridge University Press.
46. Zhao, Z., et al., *Origami by frontal photopolymerization*. Science Advances, 2017. **3**(4).
47. Flory, P.J., *Principles of polymer chemistry*. 1953: Cornell University Press.
48. Bergman, T.L., et al., *Fundamentals of heat and mass transfer*. 2011: John Wiley & Sons.
49. Wang, Q.M., et al., *Separating viscoelasticity and poroelasticity of gels with different length and time scales*. Acta Mechanica Sinica, 2014. **30**(1): p. 20-27.

50. Ma, J., et al., *A photoviscoplastic model for photoactivated covalent adaptive networks*. Journal of the Mechanics and Physics of Solids, 2014. **70**: p. 84-103.
51. Marzocca, A.J., *Evaluation of the polymer–solvent interaction parameter  $\chi$  for the system cured styrene butadiene rubber and toluene*. European Polymer Journal, 2007. **43**(6): p. 2682-2689.
52. McKenna, G.B., K.M. Flynn, and Y. Chen, *Swelling in crosslinked natural rubber: experimental evidence of the crosslink density dependence of  $\chi$* . Polymer, 1990. **31**(10): p. 1937-1945.
53. Coleman, B.D. and W. Noll, *The Thermodynamics of Elastic Materials with Heat Conduction and Viscosity*. Archive for Rational Mechanics and Analysis, 1963. **13**(3): p. 167-178.

A finite deformation model is developed to describe the desolvation and swelling in partially photo-crosslinked polymers.



239x119mm (300 x 300 DPI)